Frontiers in Bioscience Landmark

Front. Biosci. (Landmark Ed) **2026**; 31(9): 52737
https://doi.org/10.31083/FBL52737

Original Research

Radiotherapy Reconstitutes the Collapsed miRNome of Progressive Neuroblastoma and Promotes a Favorable Tumor Evolutionary Shift

Sivasubramani Narayanan[1,†], Poorvi Subramanian[1,†], Sreenidhi Mohanvelu[1,†], Sheeja Aravindan[2], Loganayaki Periyasamy[1], Natarajan Aravindan[1,2,3,*]

[1]Department of Physiological Sciences, College of Veterinary Medicine, Oklahoma State University, Stillwater, OK 74078, USA
[2]OU Health Stephenson Cancer Center, Oklahoma City, OK 73104, USA
[3]Departments of Radiation Oncology and Pathology, University of Oklahoma Health Sciences Center, Oklahoma City, OK 73104, USA
*Correspondence: natarajan.aravindan@okstate.edu (Natarajan Aravindan)
[†]These authors contributed equally.

Academic Editor: Amancio Carnero Moya
Submitted: 9 April 2026 Revised: 10 July 2026 Accepted: 23 July 2026 Published: 3 September 2026

Abstract

Background: Progressive disease (PD) remains the dominant barrier to cure in high-risk neuroblastoma (HR-NB), driven in part by profound post-transcriptional deregulation that fuels clonal evolution, stemness, immune evasion, and therapy resistance. In this study, we define the molecular architecture of PD-associated microRNA (miR) collapse and demonstrate that radiotherapy (RT) acts as a potent post-transcriptional reprogrammer capable of reversing this trajectory. **Methods:** miRNome profiling was performed in HR-NB tumors from patients during diagnosis (Dx), intensive multi-modal clinical therapy (IMCT) defiant PD, or residual disease after incorporating RT with IMCT (RD-RT). miRs' expression profiles were validated with selective miR-320a, miR-423, miR-483-3p, miR-122-5p, miR-3184-5p, miR-21-5p qPCR. RT-influenced changes in cell-identity were investigated by assessing histomorphological alterations (H&E) and multiplex immunofluorescence (mIF) for Ki-67, PD-L1, SOX2, CD44 or p53. **Results:** IMCT-defying PD displayed a loss of 167 miRs, and none upregulated, corresponding an evolutionary fingerprint for pathways governing cancer stem cell (CSC) maintenance, epithelial to mesenchymal transition (EMT), metabolic rewiring, proliferative fitness, and immune suppression. Strikingly, adding RT reversed 146 of these miRs and induced additional 179 RT-specific miRs, restoring regulatory networks governing apoptosis, p53-mediated DNA-damage response, differentiation/mesenchymal to epithelial transition (MET), and immune visibility. Individual miR-qPCR analysis of miR-320a, miR-483-3p, miR-3184-5p miR-21-5p, and miR-122-5p validated and corroborated the array expression outcomes. Histologic and mIF remarkably substantiated these miR signatures, showing that RT transforms poorly differentiated, plastic, PD-L1^{+}/SOX2^{+}/CD44^{+} CSC-like PD tumors into differentiated, lineage-stabilized, immune-permissive states characterized by neuropil restoration, ganglioneuroma-like maturation, marginal yet measurable loss of SOX2/CD44, suppression of PD-L1, complete collapse of Ki-67^{+} proliferative compartments, and significant induction of p53. **Conclusion:** Collectively, our findings indicated that RT could be a global regulator of tumor state transitions, reinstating miR-mediated governance lost during PD evolution and redirecting tumor fate toward regression. Our results provide proof-of-concept evidence that RT delivers powerful molecular benefits beyond local control, introducing a conceptual framework for miR-guided RT personalization, biomarker development, and rational combination strategies to improve outcomes in HR-NB.

Keywords: high-risk neuroblastoma; disease progression; radiotherapy; microRNAs; neoplastic cell transformation

1. Introduction

High-risk neuroblastoma (HR-NB) remains a major cause of childhood cancer mortality despite intensive multimodal clinical therapy (IMCT) [1,2]. Nearly half of patients present with HR-NB, and approximately 50% of these develop therapy-defying progressive disease (PD), leading to high relapse rates and poor survival outcomes [3]. Although IMCT integrates chemotherapy, surgery, stem-cell transplantation, immunotherapy, and differentiation therapy [3,4,5], its ability to prevent PD remains limited [6] leading to >60% relapse and dismal long-term outcomes [7,8]. PD evolution is driven by therapy-pressure steered molecular alterations that promote clonal selection, dedifferentiation, stemness, and pluripotency maintenance [9]. A critical and unresolved question is whether radiotherapy (RT), beyond its established role in local tumor control, can fundamentally alter the molecular trajectory of therapy-resistant NB and suppress PD evolution.

RT is routinely incorporated into HR-NB treatment, particularly during consolidation, where it contributes to improved local control and survival [10,11,12]. However, its mechanistic impact on PD-NB biology remains poorly defined. Increasing evidence suggests that PD evolution is driven by therapy-induced molecular reprogramming, including alterations in microRNA (miR) networks that regulate proliferation, differentiation, stemness, and metastasis [13,14,15]. While RT is known to influence transcriptional responses through DNA damage

Copyright: © 2026 The Author(s). Published by IMR Press.
This is an open access article under the CC BY 4.0 license.

Publisher's Note: IMR Press stays neutral with regard to jurisdictional claims in published maps and institutional affiliations.

and stress signaling pathways [16,17,18,19,20,21,22], its effects on post-transcriptional regulation, particularly the global miRNome, have not been systematically investigated in NB, representing a significant gap in understanding. In this study, we address this gap by performing global miRNome profiling of stage-4 HR-NB tumors to determine how RT influences PD-associated molecular evolution. We compared miR expression patterns across three conditions: tumors at diagnosis (Dx), PD tumors arising after IMCT alone, and residual tumors from patients treated with IMCT plus RT (RD-RT). This design enables a direct assessment of RT-driven molecular reprogramming under therapeutic pressure and allows identification of PD-specific regulatory signatures and their modulation by RT.

Our findings demonstrate that PD tumors arising after IMCT alone acquire distinct, therapy-driven miR signatures associated with aggressive disease evolution. Importantly, the addition of RT induces a global reprogramming of these PD-associated miR profiles. This RT-mediated remodeling affects key biological pathways, including proliferation, differentiation, metastasis, apoptosis, immune regulation, and DNA-damage signaling. Collectively, this proof-of-concept study provides evidence that RT exerts a systemic post-transcriptional regulatory effect in HR-NB, counteracting the miR-driven mechanisms underlying PD and reshaping the molecular landscape of therapy-resistant tumors. These findings pave a mechanistic foundation for understanding how RT contributes beyond local tumor control to influence disease biology. They further support the strategic integration of RT into HR-NB treatment paradigms, potentially extending its role to suppress relapse and improve long-term outcomes in patients with therapy-resistant disease.

2. Materials and Methods

2.1 NB Clinical Biospecimen Collection, Cohort Composition, and Patient Demographics

For miRNome profiling, clinical biospecimens from nine cases of human NB were collected from University of Oklahoma Health Sciences Center (OUHSC) pediatrics pathology collection. All protocols were approved by the OUHSC (IRB-14601) and Oklahoma State University (OSU, IRB-23-496) Institutional Review Boards (IRBs), permitting the research use of de-identified human specimens. All experimental procedures adhered to institutional guidelines for the protection of human subjects. To evaluate the predictive and prognostic significance of miRs in response to RT, we conducted a retrospective analysis of stage-4 HR-NB clinical cohorts comprising: (i) tumors collected at diagnosis (Dx; n = 3), (ii) progressive disease tumors from patients who failed IMCT without receiving RT (PD; n = 3), characterized by extensive dissemination, recurrence, and poor outcomes, and (iii) residual disease (RD) tumors following IMCT complemented with RT (RD-RT; n = 3). These RT-treated patients received fractionated external beam RT (EBRT) at 200 cGy/day, delivered four days per week over three weeks, to a total dose of 2400 cGy. Detailed demographic and clinical characteristics for each patient, including age, sex, MYCN (V-Myc Avian Myelocytomatosis Viral Oncogene Neuroblastoma Derived Homolog) status, International Neuroblastoma Staging System (INSS) stage, treatment history, time of specimen collection, tumor site, disease status (PD *vs.* RD), relapse history, survival, and RT exposure, are provided in Tables 1,2. To assess the adequacy of the sample size, a post hoc statistical power analysis was performed using G*Power software (Düsseldorf, North Rhine-Westphalia, Germany). Based on the study design with n = 3/group, the achieved statistical power was 61.92% (**Supplementary Fig. 1**). Formalin-fixed paraffin-embedded (FFPE) tumor specimens were obtained from institutional pediatric pathology archives. To ensure rigor and reproducibility, strict inclusion criteria were applied, and samples with insufficient tissue, poor histologic quality (e.g., tears, folds, processing artifacts), or missing essential clinical or pathological information were excluded.

2.2 miRNome Profiling

Total RNA was extracted from FFPE tissue using the RNAstorm FFPE RNA Extraction Kit (Cell Data Sciences, Fremont, CA, USA), which effectively removes formaldehyde-induced damage and markedly improves the recovery of amplifiable RNA. All steps were performed according to the manufacturer's protocol. Briefly, four FFPE sections (4.0 µm each) were deparaffinized in 500 µL of dewaxing solution at 56 °C for 5 minutes, followed by tissue precipitation (12,000 ×g for 5 minutes) and drying at 37 °C for 10 minutes. For uncrosslinking and lysis, the dried tissue was incubated in 80 µL of FFPE CAT5™ reagent at 72 °C for 30 minutes, cooled on ice for 1 minute, and then mixed with 80 µL of FFPE Lysis Buffer and 10 µL of FFPE Protease, followed by incubation at 72 °C for 2 hours. After a 3-minute of ice incubation, lysates were centrifuged at 16,000 ×g for 15 minutes, and the supernatant was transferred to a tube containing 310 µL of RNA MagBeads. The mixture was incubated for 10 minutes at room temperature and placed on a magnetic rack for ~5 minutes to allow bead capture. Beads were washed twice with 1 mL of 80% ethanol (30 seconds each, room temperature) and air dried for 5 minutes. DNA was removed by treating beads with 70 µL of DNase Buffer containing 2 µL of DNase I at 37 °C for 15 minutes, followed by addition of 105 µL of RNA Bead Buffer. After 10 minutes on a magnetic rack at room temperature, the supernatant was discarded, and beads were washed twice with 1 mL of 80% ethanol, then dried for 3–5 minutes. Purified RNA was eluted in 50 µL of RNase-free water (10 minutes, room temperature), and the RNA concentration was quantified using the RNA 6000 Nano assay on the Agilent 2100 Bioanalyzer (Agilent Technologies Inc, Santa Clara, CA, USA), and the quality was veri-

Table 1. Patient demographics and clinical characteristics.

Total cases	n = 9	
Gender	Male (n = 6)	Female (n = 3)
Age	<2Y or =2Y (n = 2)	>2Y (n = 7)
MYCN status	Amplified (n = 6)	Non-Amplified (n = 3)
INSS stage	4	
Tumor location	Adrenal (n = 5)	Abdomen (n = 4)
Relapse	No relapse = 5	Relapse = 4
Survival	Live = 7	Dead = 2
Disease status	Dx (n = 3)	PD (n = 3) RD-RT (n = 3)
Radiotherapy	Given (n = 3)	Not given (n = 6)

Summary of demographic and clinical characteristics, including gender, age at diagnosis, MYCN status, INSS stage, tumor location, relapse, survival, disease status, and RT administration. Dx, diagnostic tumors; PD, IMCT defiant progressive disease without RT; RD-RT, residual disease after IMCT with RT; INSS, International Neuroblastoma Staging System; IMCT, intensive multimodal clinical therapy; RT, Radiotherapy.

Table 2. Patient-specific clinical, pathological, and treatment characteristics.

Patients	Sex	Age at sampling (Months)	Sampling time	Primary site	Stage	Clinical status	MYCN status	CT	CT cycles	RT	RT dose (cGy)
1	M	43	5/21/1998	Adrenal gland	4	Dx	1	No	0	No	0
2	F	16	6/28/2002	Adrenal gland	4	Dx	1	No	0	No	0
3	M	33	9/24/2010	Abdomen	4	Dx	2	No	0	No	0
4	F	16	7/9/2004	Adrenal gland	4	RD	1	Yes	4	Yes	2400
5	M	83	4/26/2005	Adrenal gland	4	RD	1	Yes	1	Yes	2400
6	M	48	12/29/2011	Abdomen	4	RD	2	Yes	4	Yes	NA
7	M	42	6/21/2013	Abdomen	4	PD	2	Yes	3	No	0
8	M	60	10/16/2012	Adrenal gland	4	PD	1	Yes	4	No	0
9	F	57	10/30/2015	Abdomen	4	PD	1	Yes	3	No	0

Demographic, clinicopathological, and therapeutic variables for HR-NB patients included in this study. Variables include sex, age, date of tissue acquisition, tumor site, disease stage, disease status at the time of sampling, and MYCN genomic status (1 = amplified; 2 = non-amplified). Treatment annotations comprise chemotherapy exposure, total number of chemotherapy cycles administered, radiotherapy status, and cumulative radiation dose (cGy). The cohort includes diagnostic (Dx), progressive disease (PD), and post-radiotherapy residual disease (RD) specimens. NA indicates data not available. M, Male; F, Female; CT, Chemotherapy; RT, Radiotherapy.

fied for array performance as per the OUHSC-Stephenson Cancer Centre-CORE standards. miRNome profiling was performed using the Human miRNA OneArray® V7 platform (Phalanx Biotech, Belmont, CA, USA), which contains 2548 unique miRNA probes and 124 experimental control probes. Each probe is represented in triplicate and reflects 100% of the Sanger miRBase v18 catalog. Isolated small RNA (500 ng) was Cy5-labeled using the Kreatech ULS miRNA Labeling Kit, purified with KREApure dye-removal columns, assessed for labeling efficiency, and hybridized to the equilibrated OneArray V7 microarray at 37 °C for 16 hours following the manufacturer's protocol (Leica Biosystems, Deer Park, IL). After hybridization, arrays were sequentially washed (2× SSC/0.2% SDS → 2× SSC → 0.2× SSC), dried, and scanned using the Agilent G2600D microarray scanner (Agilent Technologies, Santa Clara, CA, USA). Raw signal intensities were quantified using ImageQuant software (GE Healthcare Bio-Sciences, Pittsburgh, PA, USA). The complete expression matrix and metadata for all miRNAs are provided in **Supplementary Material 1**.

Expression profiles of each feature were background-subtracted and normalized to internal U6 features. Phalanx recommended internal control, U6 snRNA was used as normalization control for Human miRNA OneArray platform. U6 is the widely utilized normalization control for tissue-based miRNA profiling, including FFPE sections. To eliminate inter-patient variations and identify miRs consistently altered across disease states we adopted traverse analysis (Fig. 1). For this, expression profile of background subtracted and array-normalized miRs in each patient was individually compared between Dx tumors → PD tumors; Dx tumors → RD(RT) tumors; and PD tumors → RD(RT) tumors. For differential expression miR (DEM) analysis, miRNome two-stage linear multiple comparisons were performed, and volcano plots were constructed for each group

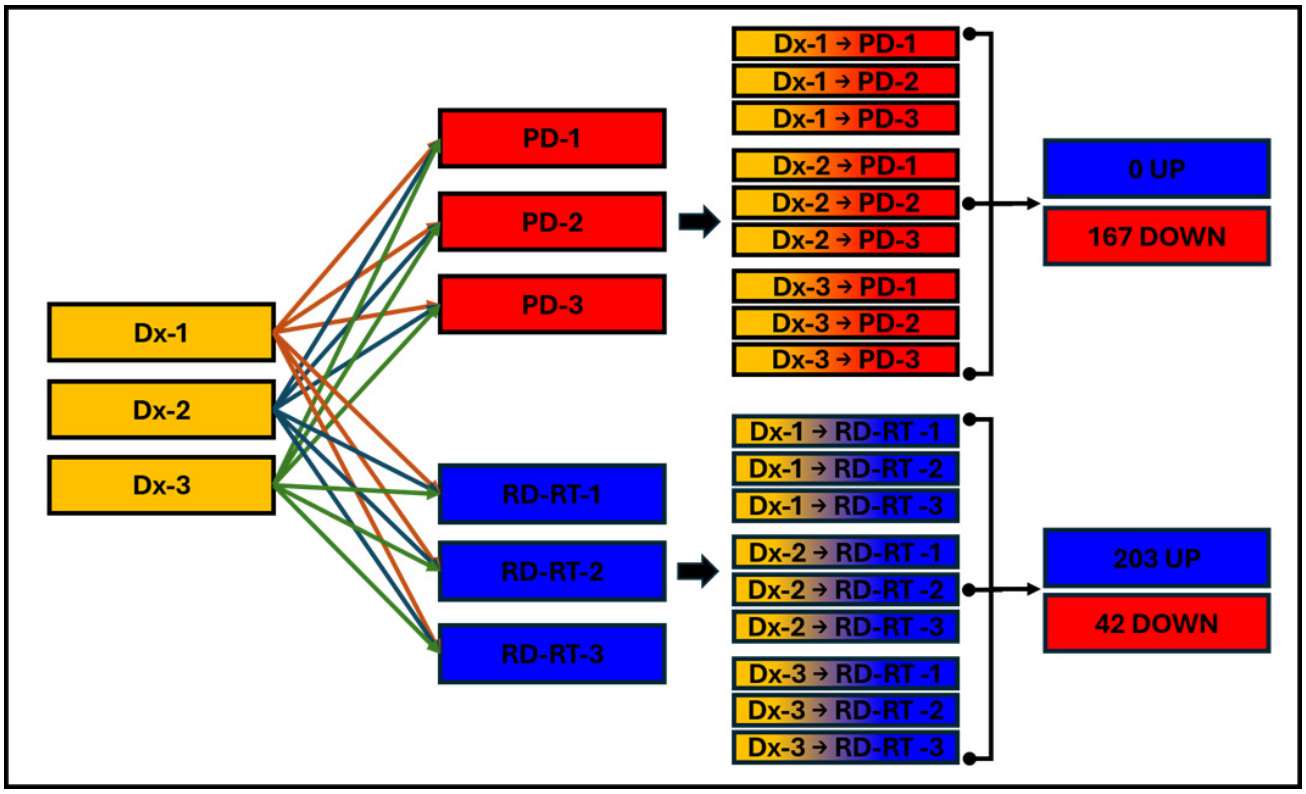


Fig. 1. Schema showing the traverse analysis workflow. Normalized miRNA expression profiles from patients derived during diagnosis (Dx) were individually compared to patients with progressive disease (PD), and residual disease following RT (RD-RT). This strategy identified miR signatures associated with disease progression and those with RT, while minimizing the inter-patient variability. Comparitive analysis revealed a notable in decrease of miRs PD, characterised exclusively by the loss of 167 miRs (0 upregulated), whereas RT resulted in the gain of 203 miRs and downregulation of 42 miRs.

comparison. The two-tier differential expression significance filter was applied, in which miR profiles were ranked based on FDR-adjusted significance [$-\log_2$(q value)] and corresponding absolute $\log_2$ FC values. miRNAs exhibiting bidirectional changes exceeding $\log_2$ FC of ±2.0 ($\log_2$FC $\geq$2.0; $\log_2$FC $\leq$–2.0) with $-\log_2$(padj) $\geq$2 were classified as statistically significant, differentially (up/down regulated) expressed. Conserved reorganized miRs with disease progression or with RT are subjected to functional enrichment analyses using miRNet 2.0, a miR-centric network visual analytics platform (https://www.mirnet.ca/upload/MirUploadView.xhtml). Analytic parameters (species, tissue type, mir-ID, gene targets) were carefully considered, and the functional enrichment assessment wasfocused on defining altered biological processes, molecular functions, and canonical pathways. To avoid false-positive results, we utilized miRNet's built-in empirical sampling and genome randomization framework to generate a robust statistical background for enrichment testing.

qPCR: We used real-time qPCR to validate the expression of selected miRs identified through miRNome profiling, including hsa-miR-320a, hsa-miR-423, hsa-miR-483, hsa-miR-122-5p, miR-3184-5p and hsa-miR-21-5p, as described in our earlier studies [23]. The qPCR validation cohort consisted of 6 patients from the Dx, 4 patients from PD, and 2 patients from the RD-RT. In brief, total RNA was polyadenylated using Poly(A) Tailing Kit (Life Technologies, Grand Island, NY, USA) followed by cDNA synthesis (miRNA EasyScript™ cDNA Synthesis Kit, Applied Biological Materials, Richmond, BC) according to the manufacturer's instructions. hsa-miR-U6 served as the internal control for normalization. miR expression was calculated using U6-normalized $^{\Delta\Delta}$Ct values. Relative changes in miRNA expression were determined by comparing PD and RD-RT tumors to their matched Dx tumor samples using the $^{\Delta\Delta}$Ct approach. Data are presented as FC, calculated from the $^{\Delta\Delta}$Ct values. Group-wise comparisons were performed using two-way ANOVA followed by Tukey's post-hoc correction in GraphPad Prism v10.1.0 (GraphPad software Inc, La Jolla, CA, USA).

2.3 Histology, Multiplex Immunofluorescence, Digital Microscopy, Imaging and Quantification

All histology and multiplex IF studies were performed in the COBRE-Cancer Tissue Pathology Core of OU-Health Stephenson Cancer Center following standard protocols, as described in our prior studies [15,23]. Tissue sections were subjected to hematoxylin and eosin (H&E) stain-

ing for histopathological evaluation. Briefly, sections were deparaffinized, rehydrated through graded ethanol, and stained using standard H&E protocols. Whole-slide sections with intact and representative tumor architecture were used for histological assessment to evaluate RT-associated morphological alterations, including cellular differentiation status, nuclear morphology, neuropil formation, ganglion-like differentiation, and stromal remodeling. Comparative analyses between RT and mock exposure were performed to define features consistent with RT-associated tumor maturation and therapeutic benefit in NB. Multiplex-IF was performed as described in our previous studies to characterize RT-regulated protein networks linked to miR-mediated signaling [24]. In brief, automated multiplex-IF was performed on the Leica Bond RX using the opal 5-color automated IF kit (Akoya Biosciences, Marlborough, MA, USA) following the manufacturer's protocol. For this, 4 µm thick tissue sections were dried (overnight at room temperature), baked (60 °C for 45 min), deparaffinized and treated for target retrieval (100 °C for 20 min). Automated multiplex-IF staining was carried out on a Leica Bond RX autostainer using the Opal multiplex IF system (Akoya Biosciences, Marlborough, MA, USA) following the manufacturer's instructions. For this study, we used mouse monoclonal rabbit polyclonal anti-SOX2 (Aviva systems biology, San Diego, CA, USA), rabbit monoclonal anti-PD-L1 (Cell Signaling, Danvers, MA, USA), mouse monoclonal anti-Ki-67 (LS Bio, Newark, CA, USA), anti-CD44 (Cell Signaling, Danvers, MA, USA), and anti-p53 (Abcam, Waltham, MA, USA) antibodies. For fluorescence detection, opal polymer HRP Ms+Rb conjugate and detection substrate (Opal 520, Opal 570, Opal 620, Opal 690 and Opal 780) was utilized. Nucleus was counterstained with Spectral DAPI, the slides were mounted with Prolong Gold antifade reagent (Invitrogen, Waltham, MA, USA), cured for 12 h and scanned within 48 hours using Zeiss Axioscan.Z1 (Carl Zeiss Mircoscopy LLC, White Plains, NY, USA) with calibre7 at 40× magnification. Critically, RT-associated tumor cell phenotypes were characterized as PD-L1^{+}, CD44^{+} plasticity-associated, SOX2^{+} CSC-like, proliferating (Ki-67^{+}), and/or DNA damage response (p53^{+}) tumor cells.

3. Result

3.1 Therapy-Defying NB-PD Harbors a Distinct, Disease-Evolution-Focused miR Fingerprint

To define the miR footprint of therapy-defying NB-PD and to determine how it differs from therapy-naïve tumors at Dx, we identified statistically significant miR alterations using combined $\log_2$ FC ≤ -2 and $-\log_2$(padj) ≥ 2 criteria. Compared with Dx tumors, PD tumors exhibited exclusive downregulation of 167 miRs with no corresponding miR gains, representing a distinct and uniform PD-associated miR-loss signature (Figs. 2A,3,4). Functional mapping of these PD-suppressed miRs revealed extensive, tumor-evolution–focused molecular rewiring, significantly ($p < 0.05$) impacting 96 canonical pathways (214 total altered), with cancer progression being the most enriched ($p = 5.73 \times 10^{-13}$). Key signaling networks involved in tumor evolution, including Jak-STAT, Notch, T-cell receptor, Hedgehog, NOD-like receptor, B-cell receptor, neurotrophin, ErbB, MAPK, p53, phosphatidylinositol, Wnt, RIG-I-like receptor, insulin, mTOR, apoptosis, TGF-β, and GnRH pathways, were significantly disrupted (**Supplementary Material 2, Sheet 1**). These pathway-level disruptions significantly ($p < 0.05$) altered 74 cellular processes (224 total), including the microtubule-organizing center, RNA polymerase II complexes, PML-body formation, Golgi membrane integrity, ubiquitin ligase complexes, replication fork stability, HDAC complexes, and ribonucleoprotein assembly (**Supplementary Material 2, Sheet 2**). Correspondingly, 71 biological functions (378 total) were substantially ($p < 0.05$) perturbed, spanning ATP binding, chromatin remodeling, kinase and GTPase activity, SH3-domain interactions, ubiquitination, SMAD binding, transcriptional regulation, and protein transport (**Supplementary Material 2, Sheet 3**). Collectively, this tightly integrated cascade, signaling pathway → cellular process → biological function, demonstrates that IMCT-induced miR-loss directly promotes gain-of-function phenotypes associated with tumor evolution, including epithelial to mesenchymal transition (EMT), mesenchymal stem-cell proliferation, NK-cell modulation, glucose/lipid/cholesterol metabolism, autophagy, DNA damage repair, T-cell differentiation, cell motility, and immune evasion (**Supplementary Material 2, Sheet 4**). Importantly, the PD-miR signature parallels molecular footprints observed in other highly aggressive solid tumors such as prostate, renal, pancreatic, small-cell lung, colorectal, endometrial, non-small-cell lung, brain, and bladder cancers. Taken together, these differential expression analyses and functional enrichment data suggest that IMCT-driven miR loss contributes to progressive NB biology, facilitating therapy resistance, immune escape, EMT, clonal selection, plasticity, stemness maintenance, self-renewal, and metastatic competence. In comparison with Dx tumors, NB-PD harbors a direct and distinct post-transcriptional signature of tumor evolution shaped by therapy pressure.

3.2 Clinical RT Completely Annuls IMCT-Pressure-Driven miR Loss in NB-PD

To determine whether adding RT to the treatment regimen for HR-NB can stabilize or reverse the IMCT-pressure-associated loss of 167 miRs, we evaluated miRNome changes in PD tumors from patients who received IMCT with RT. Remarkably, RT produced a reversal of 146 of the 167 PD-associated lost miRs, with 142 miRs exhibiting robust ($\log_2$FC ≥ 2) upregulation (Figs. 3,4). Among these, 24 miRs, including *hsa-miR-4430*, *hsa-miR-4723-5p*, *hsa-miR-6721-5p*, *hsa-miR-638*, *hsa-miR-6732-5p*, *hsa-miR-5196-5p*, *hsa-miR-7977*, *hsa-miR-3178*, *hsa-*

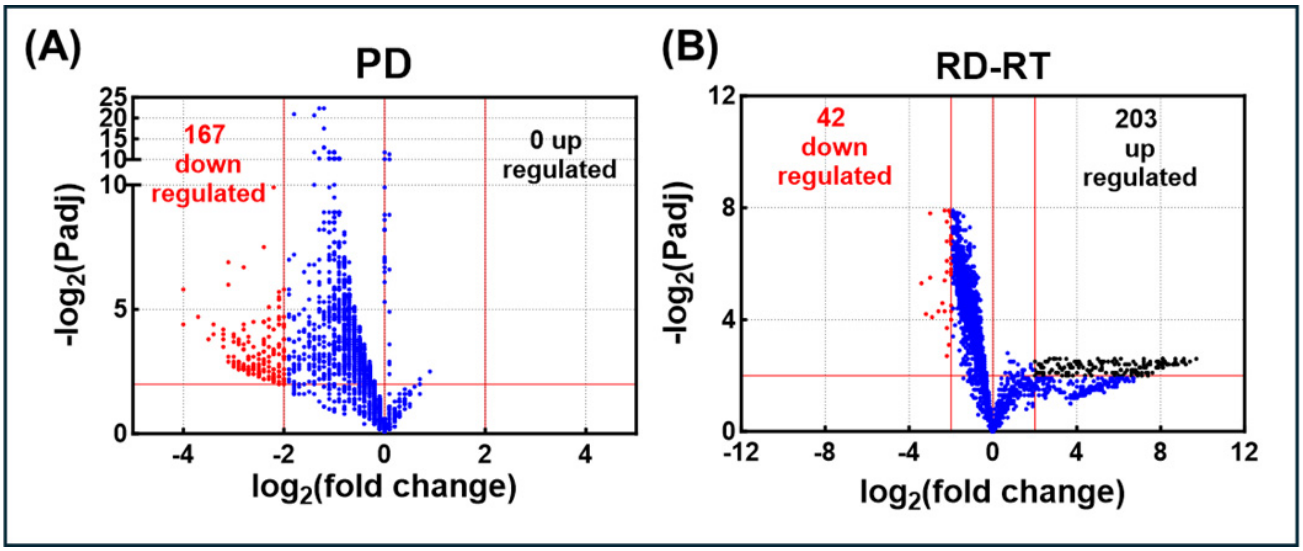


Fig. 2. miR landslides in NB disease progression and RT. Differential miR expression analysis from miRNome profiling displaying (A) significant downregulation of 167 miRs with none upregulated in the IMCT defiant PD group, and (B) adding RT to the treatment associated reprogramming of miR landscape, with 203 upregulated and 42 downregulated miRs. Significance thresholds were defined as $-2 \geq \log_2$ (Fold Change) ≥ 2 with FDR corrected log (padj) ≥ 2 using GraphPad Prism v10.1.0.

miR-6825-5p, *hsa-miR-3665*, *hsa-miR-4649-5p*, *hsa-miR-4419b*, *hsa-miR-6746-5p*, *hsa-miR-7107-5p*, *hsa-miR-937-5p*, *hsa-miR-6785-5p*, *hsa-miR-1909-3p*, *hsa-miR-6763-5p*, *hsa-miR-4507*, *hsa-miR-6858-5p*, *hsa-miR-513a-5p*, *hsa-miR-6824-5p*, *hsa-miR-6885-5p* and *hsa-miR-494-3p* showed robust induction, meeting both $\log_2$ FC ≥ 2 and $-\log_2$(padj) ≥ 2 thresholds (Figs. 3,4). Although 21 miRNAs remained downregulated despite RT exposure, only nine, *hsa-miR-4743-3p*, *hsa-miR-5089-3p*, *hsa-miR-190b*, *hsa-miR-3165*, *hsa-miR-148a-5p*, *hsa-miR-129-1-3p*, *hsa-miR-4633-3p*, *hsa-miR-598-5p*, and *hsa-miR-6772-3p*, were consistently and significantly suppressed [log2 FC ≤ -2 and $-\log_2$(padj) ≥ 2]. The remaining 12 miRs that showed downregulation both with and without RT exhibited attenuated loss in the presence of RT without statistical significance, further reflecting RT's stabilizing influence on the miRNome (Fig. 3). Collectively, these findings demonstrate that RT effectively counteracts IMCT-driven miR collapse, restoring a broad regulatory repertoire lost during PD evolution. By alleviating miR depletion linked to therapy resistance, immune evasion, EMT, clonal selection, cellular plasticity, stemness maintenance, self-renewal, and metastatic competency, RT re-establishes critical tumor-suppressive post-transcriptional controls. These findings suggest that RT exerts effects beyond local tumor control, potentially reprogramming molecular pathways capable of reversing PD-associated evolutionary advantages.

3.3 RT Programs De Novo miR Gains That Repress the Evolution of PD-NB

To further determine whether RT autonomously rewires the miRNome to drive antitumor responses in PD-NB, we compared RT-treated PD tumors with those exposed to IMCT alone. Adding RT resulted in a de novo gain of 179 miRNAs, each meeting stringent thresholds of $\log_2$ FC ≥ 2 and $-\log_2$(padj) ≥ 2 (Figs. 2B,4,5). Functional enrichment of these RT-induced miRs revealed significant ($p < 0.05$) modulation of 92 canonical pathways (214 total altered), with "pathways in cancer" remaining the most prominently regulated ($p = 8.01 \times 10^{-11}$). Notably, RT reprogrammed multiple overlapping signaling networks central to tumor evolution, including aminoacyl-tRNA biosynthesis, purine/pyrimidine metabolism, FcγR-mediated phagocytosis, N-glycan biosynthesis, endocytosis, protein processing in the endoplasmic reticulum, focal adhesion, ErbB, MAPK, insulin, p53, Wnt, RIG-I–like receptor, Jak-STAT, Notch, mTOR, neurotrophin, TGF-β, phosphatidylinositol, T-cell and B-cell receptor signaling, NOD-like receptor signaling, apoptosis, and GnRH pathways (**Supplementary Material 3, Sheet 1**). These pathway changes significantly altered 67 cellular processes (224 total), including PML-nuclear body formation, RNA polymerase complexes, adherens junctions, ubiquitin-ligase complexes, replication forks, spliceosomal assemblies, microtubule-organizing centers, HDAC complexes, transcription factor complexes, and serine/threonine phosphatase complexes (**Supplementary Material 3, Sheet 2**). Correspondingly, 70 biological functions (378 total) were modified, spanning MAPKKK activity, ligase and transporter functions, RNA polymerase and transcription corepressor activity, nucleotide metabolism, protein-domain interactions, chromatin remodeling, kinase and Ras-GTPase activities, HDAC interaction, zinc-ion and damaged-DNA binding, ubiquitination, phosphatase and phospholipid binding, and

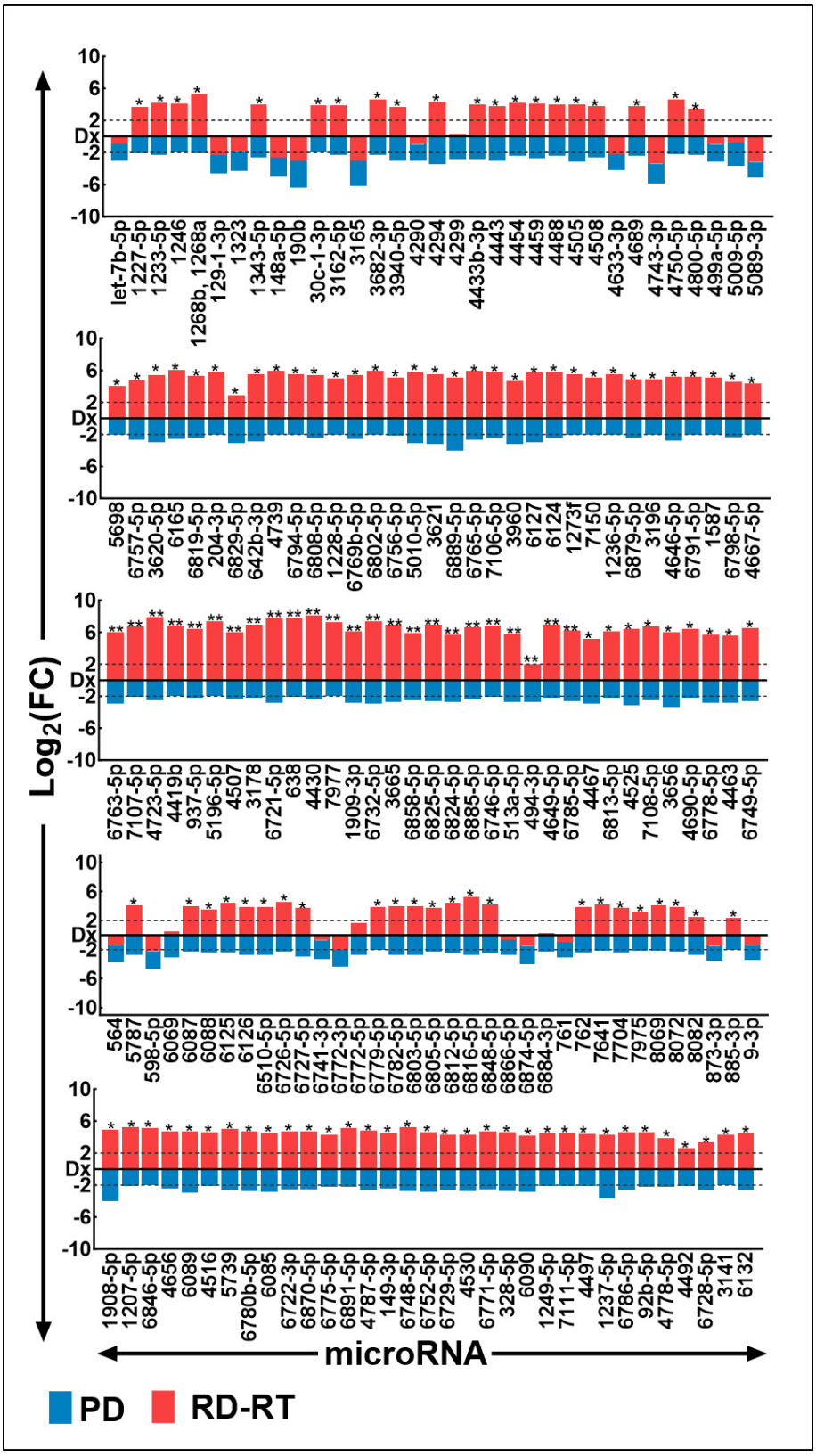


Fig. 3. Therapy pressure reshaped miR landscape in NB. Histograms from miRNome analysis showing significant (log_2 FC, log_2 Padj) suppression of 167 miRs in therapy defiant progressive disease (PD) when compared with disease at diagnosis (Dx). These therapy pressure associate diminutions of 146 miRs were reversed with the addition of RT to the therapy (RD-RT). *FC significant; **Both FC and Padj significant. FC, Fold change; Padj, P adjusted value. Blue bars indicate changes miR expression in PD relative to matched Dx, and red bars indicate changes in RD-RT relative to Dx.

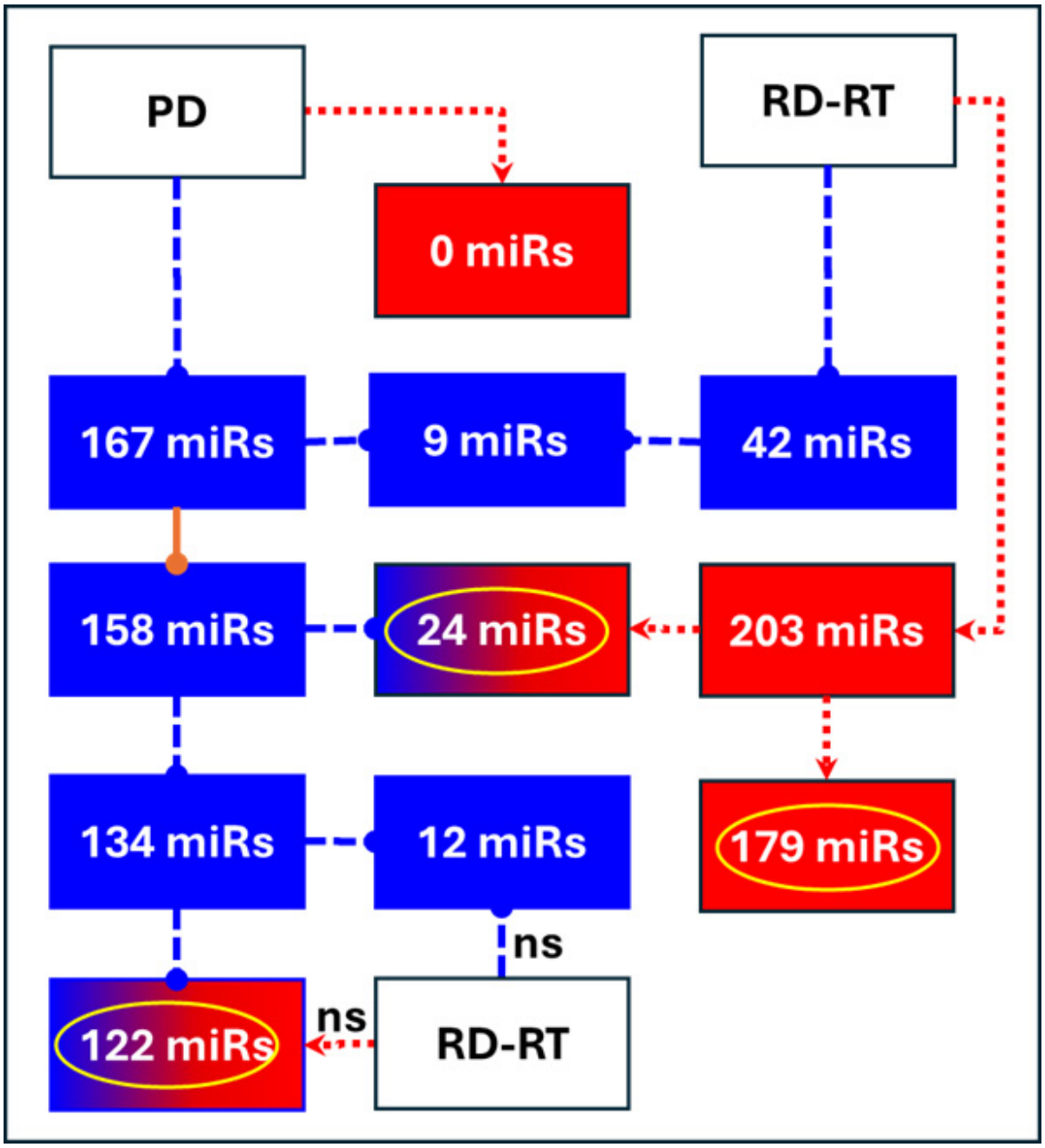


Fig. 4. miRNome modifications in the therapy defiant NB tumors with and without addition of RT treatment. Flow diagram showing the number of miRs significantly (FDR: Log_2 FC+Log_2 Padj) altered in PD, RD-RT and the shift of PD-downregulated miRs with the addition of RT. Blue box, Downregulated; Red Box, Upregulated; blue lines, inhibited; red lines, induced; yellow rings, miRs reversed or reprogrammed by RT; ns, not significant.

mRNA-binding functions (**Supplementary Material 3, Sheet 3**). This orderly RT-driven cascade—*signaling pathway → cellular process → biological function*, produced functional outputs strongly aligned with tumor-regressive biology, including mesenchymal-to-epithelial transition (MET), lipid and glucose metabolism normalization, NK-cell activation, T-cell differentiation, enhanced apoptosis, innate immune activation, stem-cell regulation, and critically, embryonic stem-cell differentiation (**Supplementary Material 3, Sheet 4**). Collectively, these RT-activated miR programs demonstrate a consistent gain of function associated with reversal of several hallmarks of PD evolution by promoting MET, reducing CSC fitness, restoring cellular identity, and increasing immune visibility. In effect, RT emerges as a potential post-transcriptional reprogramming force that suppresses key drivers of PD-NB progression.

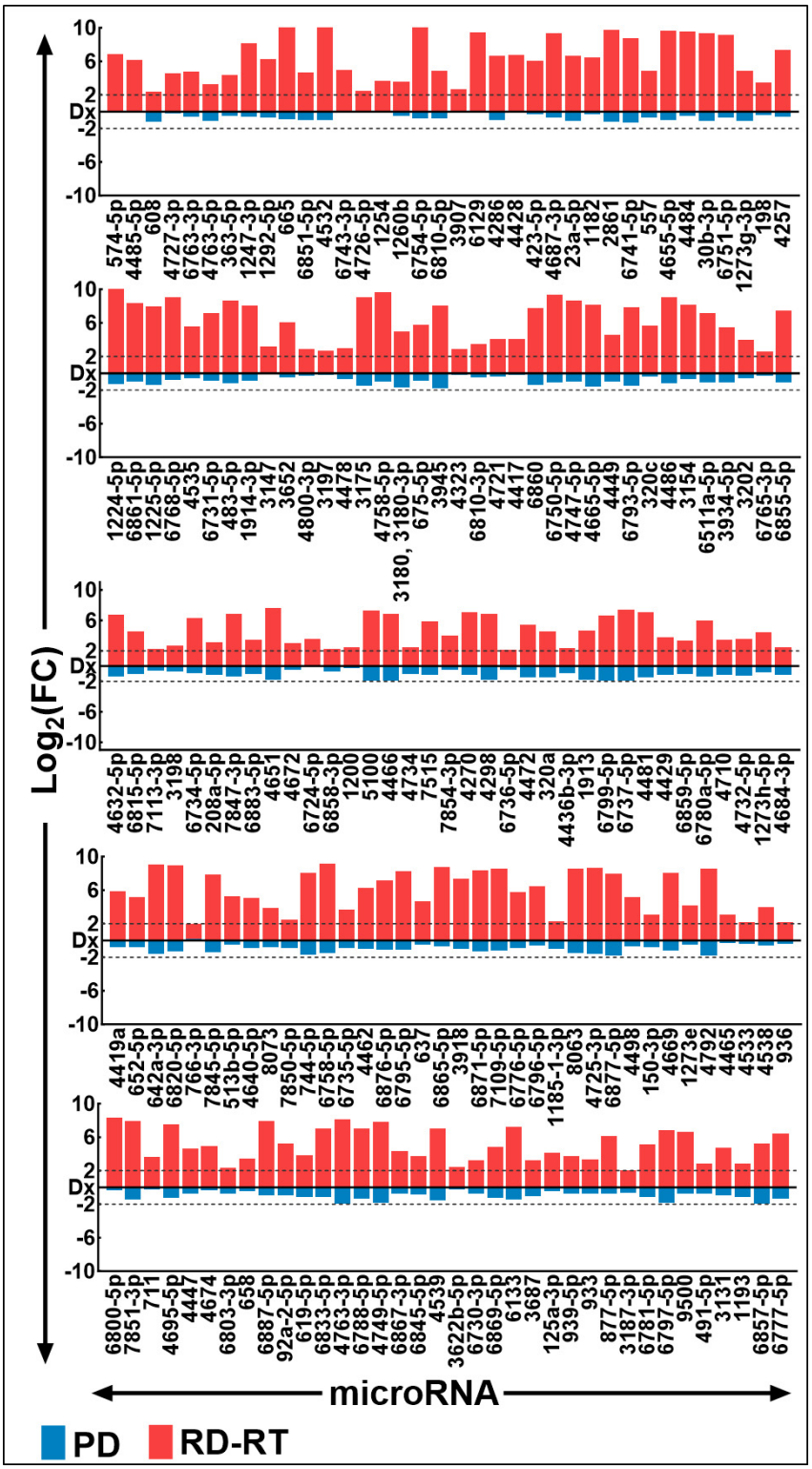


Fig. 5. RT-induced reprogramming of miR landscape in progressive NB. Histograms from miRNome analysis showing significant (log_2 FC, log_2 Padj) upregulation of 179 miRs in residual NB after addition of RT to the IMCT (RD-RT, red bars) when compared with disease at Dx. RD-RT upregulated 179 miRs were originally lost in PD (blue bars). FC, Fold change; Padj, adjusted *p* value.

3.4 Individual miR-qPCR Corroborates miRNome Modifications

To independently validate array-derived miRNome signatures associated with therapy-defying PD and the impact of RT, we examined a panel of miRs (miR-320a, miR-423, miR-483-3p, miR-122-5p, miR-3184-5p, miR-21-5p) spanning diverse trajectories across the disease continuum (Fig. 6). Collectively, these miRs encompass diverse bi-

ological functions ranging from exosome-mediated drug resistance (miR-320a), context-dependent oncogenic and tumor-suppressive signaling (miR-423), proliferative and anti-apoptotic oncogenic activity (miR-483-3p), metabolic and inflammatory regulation (miR-122-5p), suppression of oncogenic receptor signaling (miR-3184-5p), and canonical tumor-promoting functions linked to proliferation and invasion (miR-21-5p). Corroborating the miRNome profile, PD tumors displayed a clear and reproducible divergence from the Dx state (Fig. 6). Compared to Dx, miR-320a, miR-423, miR-483-3p, miR-3184-5p, and miR-21-5p was markedly reduced in PD, supporting the emergence of a coordinated post-transcriptional deregulation associated with therapy-driven disease evolution. Crucially, this shift was not confined to a single miR family or pathway but instead encompassed regulators governing diverse cellular processes, including drug resistance, tumor growth, apoptosis, receptor signaling, and cellular plasticity (Fig. 6). These findings reinforce the concept that therapy-resistant tumors undergo extensive remodeling of miR-mediated regulatory networks rather than isolated alterations in specific signaling pathways. RT on the other hand, reshaped the PD miR landscape. Notably, RT resulted in the restoration of miR-320a from its repressed state in PD (Fig. 6). Likewise, miR-483-3p and miR-3184-5p displayed marked recovery and parallels (or more) the Dx controls. Restoration of miR-3184-5p is of particular interest, given its reported tumor-suppressive role through targeting oncogenic receptor signaling pathways such as Epidermal Growth Factor Receptor (EGFR), suggesting that RT could at least in part reinstate regulatory constraints, that were lost during disease progression (Fig. 6). More importantly, majority of the miR-qPCR finding mirrors the expression profile with array and validates the miRNome modifications across the disease states and RT (Fig. 6).

3.5 RT Steers Tissue Remodeling Prompting Differentiation

To investigate the effects of RT on tumor tissue architecture, cellular differentiation, and maturation, H&E-stained tumor (FFPE) sections were compared. Disease during Dx harbored moderately differentiated NB, characterized by looser neuroblast packing, amphophilic nuclei, moderate nuclear to cytoplasmic ratios, prominent neuropil regions, and partially differentiated neuroblast cells exhibiting cytoplasmic enlargement (Fig. 7A). Conversely, PD showed poorly differentiated NB, displaying tightly packed sheets of small, round neuroblasts with hyperchromatic nuclei, high nuclear-to-cytoplasmic ratios, and scant neuropil (Fig. 7B). These morphological characteristics reflect an undifferentiated, highly proliferative state typical of aggressive NB.

However, RD revealed a remarkable architectural reorganization with enhanced differentiation and neuronal maturation. The neuroblast density was markedly decreased and accompanied by the development of extensive neuropil regions and the emergence of morphologically distinct populations of differentiating neuroblasts exhibiting enlarged cytoplasm. In several areas, mature ganglionic cells and ganglioneuroma-like regions were evident, highlighting pronounced lineage maturation (Fig. 7C). The presence of these differentiated cell types suggested that RT not only exerted cytotoxic pressure on proliferating neuroblasts but also induced phenotypic reprogramming toward a more differentiated and less aggressive state (Fig. 7C). Taken together, these findings demonstrate that RT facilitates NB maturation from a poorly differentiated phenotype toward a benign, ganglioneuroma-like composition, representing a critical morphological hallmark of treatment response.

3.6 RT-Programmable miRs Rewire Neoplastic Cell Transformation Physiology

Substantiating our RT-regulated miR footprints in therapy-defying HR-NB, we investigated whether such miR program modifications translate into measurable function on tumor cell identity and immune behavior. Given that miRs operate through coordinated attenuation of biological effects rather than single-gene effects, we performed multiplex-IF on functionally interdependent panel capturing immune evasion (PD-L1), cellular plasticity (CD44), pluripotency maintenance (SOX2), proliferative fitness (Ki-67), and DNA damage response (p53) (Fig. 8A). It is pertinent to mention that, despite their designated nuclear localization, we observed some off-site localization of Ki-67, p53 and SOX2. However, this subcellular localization of these proteins is evident in diverse cellular systems (https://www.proteinatlas.org/), while the exact cause and function remain elusive.

3.6.1 RT Attenuates miR-Linked Tumor Plasticity and CSC Programs

Cellular plasticity and CSC status are defining features of defiant PD encoded by miR-mediated control of transcriptional identity programs. Consistent with our miR signature, PD post-IMCT without RT, displayed enrichment of SOX2 relaying miR-depleted environment to CSC status and pluripotency maintenance (Fig. 8A). Consistently, CD44, a central mediator of tumor plasticity and CSC fitness, is robustly expressed in PD, often co-localizing with SOX2, indicating integrated stemness-plasticity programs under IMCT-pressure. Interestingly, RT depleted both CD44 and SOX2, potentially favoring lineage stabilization in addition to inhibiting tumor growth (Fig. 8A). Although these reductions did not reach statistical significance, the observed downward trend suggests a modest yet measurable impact on stemness-associated markers.

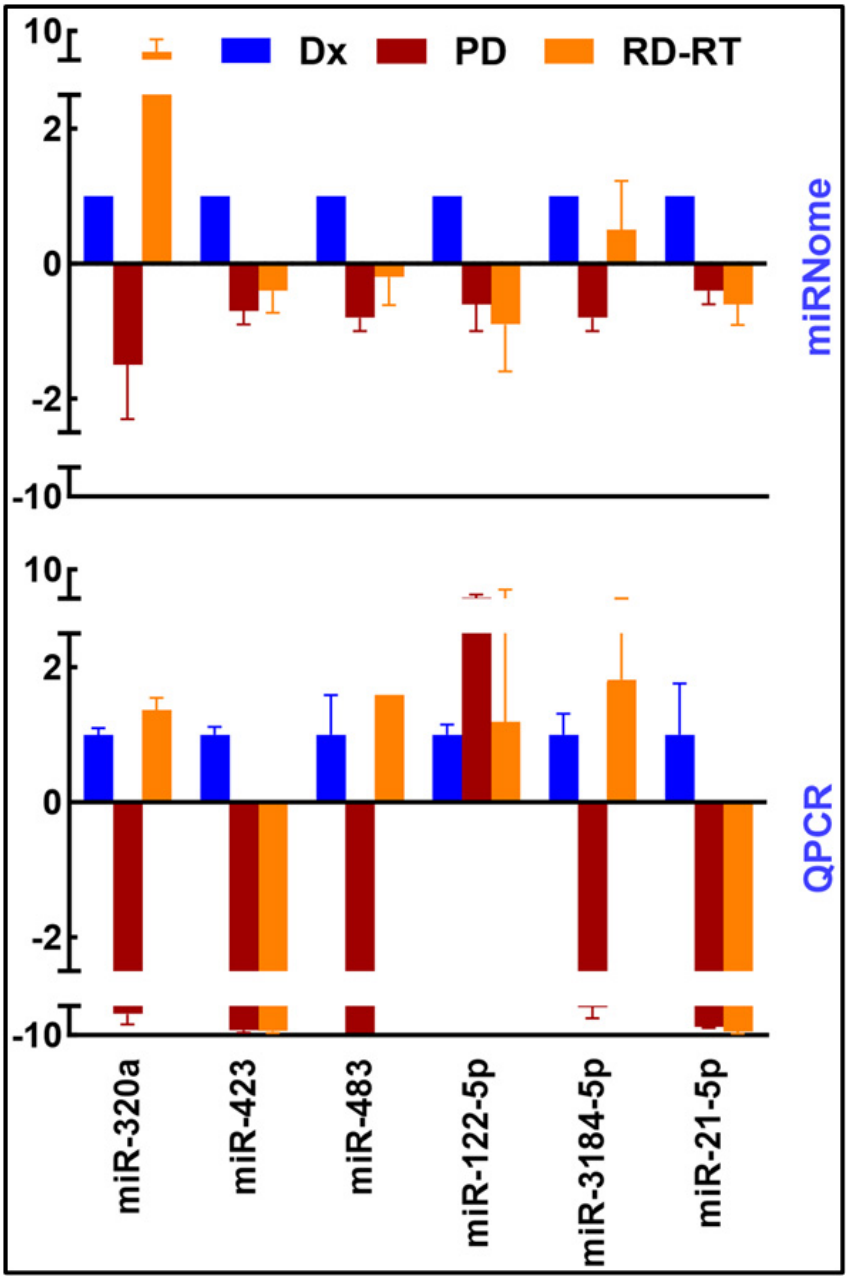


Fig. 6. RT influences progression-associated miR networks in HR-NB. Relative expression of selected progression-associated miRs identified by miRNome profiling and validated by qPCR in an expanded cohort including additional tumors of diagnostic (Dx, n = 6), progressive disease (PD, n = 4), and radiotherapy-treated recurrent tumors (RD-RT, n = 2). Upper panel shows miRNome array-derived expression changes, and lower panel shows independent qPCR validation of miR-320a, miR-423, miR-483-3p, miR-122-5p, miR-3184-5p, and miR-21-5p. PD tumors exhibited reduced expression of multiple miRs compared with Dx tumors, consistent with extensive remodeling of miRNA-mediated regulatory networks during disease progression. RT induced selective restoration of several progression-suppressed miRNAs, most notably miR-320a, miR-483-3p, and miR-3184-5p. Overall expression patterns closely mirrored the global miRNome landscape, supporting reproducible RT-induced reprogramming of post-transcriptional regulatory networks in therapy-resistant NB. Y-axis = fold change over Dx. Data are presented as mean ± SEM.

3.6.2 RT Restrains Proliferative Fitness in Tumor Cells

Uncontrolled proliferative capacity is a hallmark of malignant cells. PD displayed high number of Ki-67^{+} cells reflecting sustained proliferative fitness despite IMCT pressure. More importantly, Ki-67 positivity frequently coincided with CD44^{+} and SOX2^{+}, indicating that proliferative index was concentrated within plastic CSC subsets (Fig. 8A). Adding RT to IMCT not only reduced the Ki-67^{+} fraction, but also the concurrent induction of p53, indicating collapse of proliferative capacity and activation of stress-

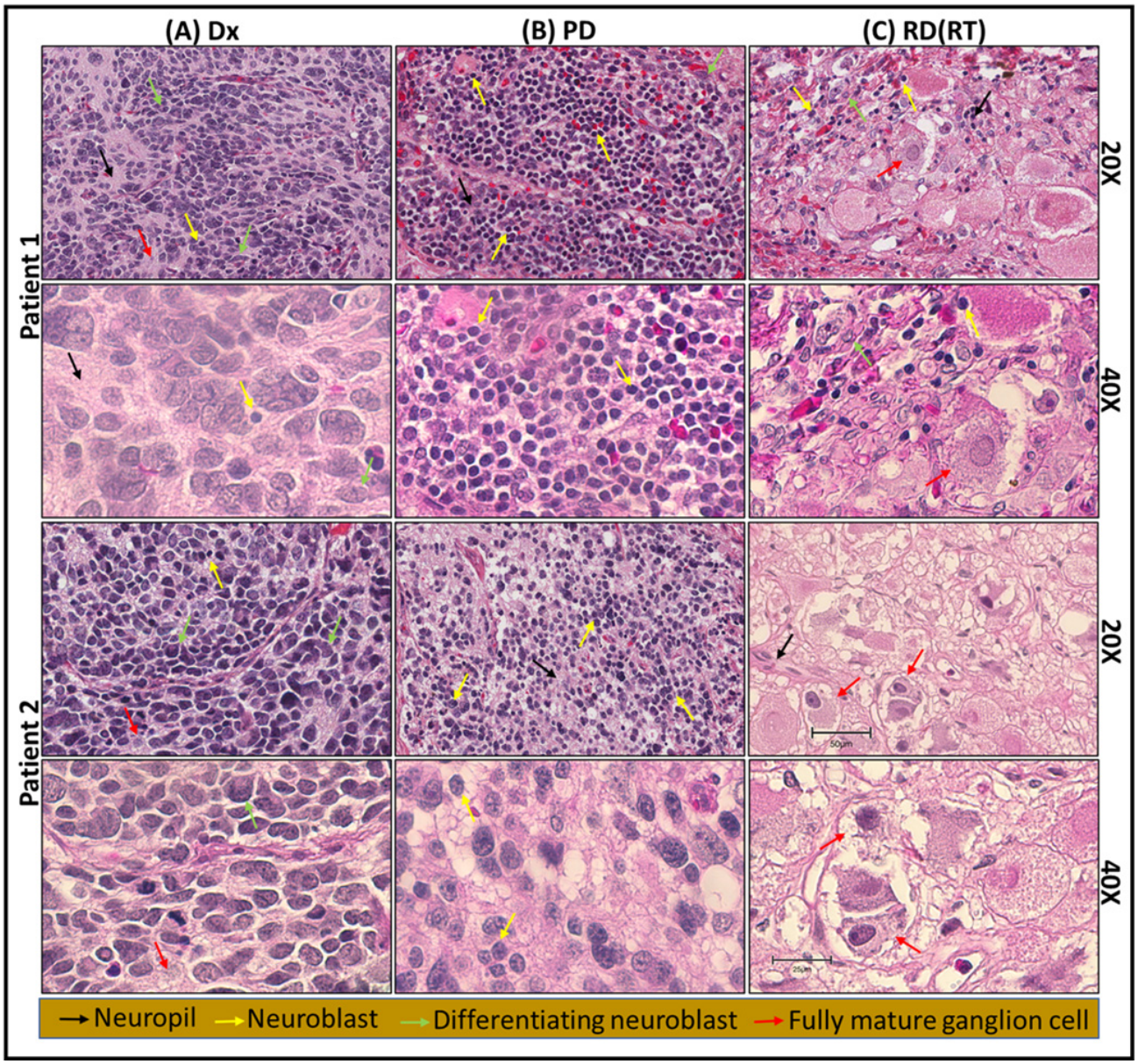


Fig. 7. Histomorphological changes in HR-NB during Dx, PD, and RD-RT. Representative H&E microphotographs of NB tissue during (A) Dx, (B) PD, and (C) RD-RT (20× and 40× magnifications; scale bar, 50 µm and 25 µm respectively) showing partial differentiation with neuropil and differentiating neuroblasts in Dx; dense neuroblast populations in PD; and differentiation with reduced neuroblast density and increased mature ganglion cells with RT. Black arrows, neuropil; yellow arrows, neuroblasts; green arrows, differentiating neuroblasts; red arrows, fully mature ganglion cells.

response and checkpoint enforcement mechanisms (Fig. 8A). These findings corroborate our miR functional enrichment analyses showing RT-mediated activation of p53 signaling, DNA damage response pathways, and apoptosis, while suppressing cell-cycle progression and replication fork instability.

3.6.3 RT Impedes Immune Evasive Programs Through PD-L1 Regulation

PD displayed robust PD-L1 upregulation, reflecting the immune-suppressive microenvironment shaped by IMCT-induced post-transcriptional deregulation (Fig. 8A). Crucially, PD-L1^{+} tumor cells frequently co-localized with CD44^{+} and SOX2^{+} tumor compartments, indicating that plastic, stem-like tumor states are preferentially selected to evade immune detection (Fig 8A). Although not statistically significant, RT resulted in a suppression of PD-L1 expression which coincided with attenuation of CD44 and SOX2, demonstrating that RT disengages immune checkpoint and the plastic tumor states that necessitate immune evasion (Fig. 8A).

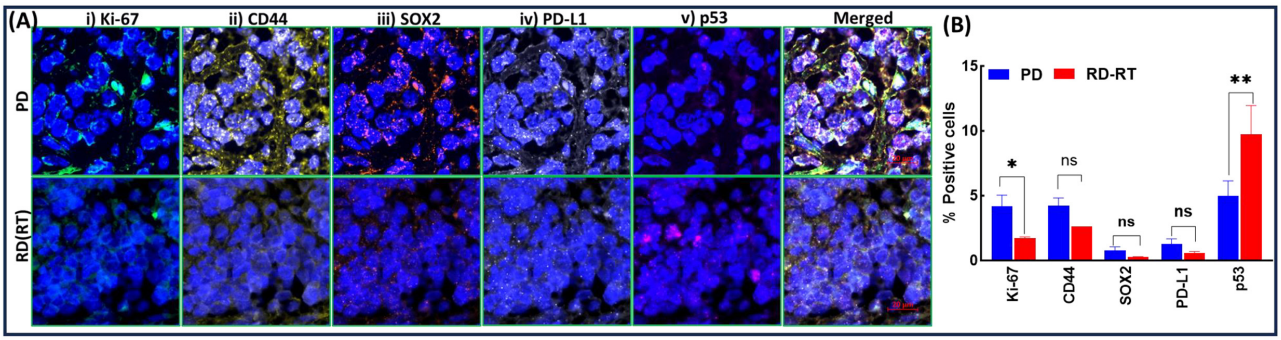


Fig. 8. RT reverts proliferation, stemness immune evasion in PD. (A) Representative microphotographs from multiplex-IF showing RT-induced changes in Ki-67, CD44, SOX2, PD-L1, and p53 in PD, when compared with PD without RT (40× magnification; scale bar 20 μm) indicating diminished replication, promoting differentiation, immune enriched states, activation of stress response and cell death programs. (B) Histogram from QuPath image analysis showed remarkable decrease in Ki-67, and robust increase of p53, While CD44, SOX2, and PD-L1 showed decreased expression, the observed reductions were not statistically significant in RD-RT (*vs.* PD). Data are presented as mean ± SEM. Statistical significance was determined using Student's *t*-test n = 2/group; *$p < 0.05$; **$p < 0.01$; ns, not significant.

Functionally, these findings align with RT-induced miR pathway enrichment for T-cell differentiation, immune signaling, and antigen-presentation processes, supporting a potential role for RT in fostering an immune-permissive tumor microenvironment. Digital quantification of mIF revealed distinct marker-specific differences between PD and RD-RT tumors (Fig. 8B). Ki-67-positive proliferating cells were significantly reduced in RD-RT compared with PD, suggesting decrease in proliferative activity following RT. p53-positive cells were significantly increased in RD-RT tumors ($p < 0.01$), indicating enhanced p53 pathway activation in the post-RT setting. Expression of SOX2, CD44, and PD-L1 showed marginal yet measurable decrease with RT treatment, suggesting that stemness and immune-checkpoint is affected by RT. Collectively, these qualitative and quantitative data support the RT-associated shift in proliferative and p53-mediated stress-response signaling.

4. Discussion

This study provides evidence that RT exerts biological effects in progressive NB that extend beyond conventional DNA damage-induced cytotoxicity. While prior studies have primarily framed RT through transcriptional responses governed by p53, ATM/ATR, MYCN, and inflammatory signaling networks, the present findings identify widespread remodeling of the miR-landscape as a previously underappreciated component of the radiation response [16,22,25,26,27,28,29,30]. The coordinated re-establishment of miR programs following RT implies that radiation may influence tumor evolution not only by eliminating malignant cells, but also by restoring regulatory mechanisms that constrain phenotypic plasticity. Such a model is particularly relevant in progressive NB, where therapeutic selection pressures favor adaptive cell states associated with stemness, lineage infidelity, treatment resistance, and immune evasion [24]. Viewed in this context, RT appears capable of re-engaging regulatory circuitry that opposes these progression-associated traits, thereby shifting the balance from adaptive survival toward more restricted and therapeutically vulnerable cellular states.

Our outcomes identified specific miRs that may serve as key nodes within this RT-responsive regulatory program. For instance, miR-320 family has been critically linked to the suppression of EMT, CSC maintenance, metastatic dissemination, and therapy resistance across multiple malignancies [14]. The prominent restoration of miR-320a with RT therefore raises the possibility that radiation not only suppresses tumor burden but also counteracts biological programs that sustain aggressive disease behavior. Given that miR-320 family members have implications in exosome-mediated communication, suggests that RT-induced miR-320a re-expression could influence both tumor-intrinsic and microenvironmental determinants of progression [14]. Although not well characterized in NB, miR-3184-5p has been implicated in the negative regulation of growth factor-driven pathways, including EGFR-associated signaling networks. Re-establishment of this regulatory axis after RT is consistent with the concept that RT can restore inhibitory post-transcriptional controls that become attenuated during disease progression. This finding is particularly relevant because receptor tyrosine kinase signaling has emerged as a major mechanism underlying therapeutic adaptation and treatment escape in HR-NB. In addition, miR-483-3p and miR-423 has been reported to function as a context-dependent regulators of proliferation, apoptosis, and stress adaptation. On the other hand, miR-122-5p occupies a central position in metabolic regulation

and inflammatory signaling. Their altered expression patterns suggest that RT-associated miR reprogramming may converge not only on intrinsic tumor cell fate decisions but also on broader processes governing metabolic fitness and interactions with tumor microenvironment. Conversely, the relatively distinct response of miR-21-5p, one of the most extensively characterized oncogenic miRs, indicated that RT may not globally normalize all progression-associated miRNA alterations. Rather, RT appears to selectively reshape specific regulatory subnetworks, reinforcing the notion that therapeutic reprogramming occurs through targeted restructuring of miR circuitry, and not the random restoration to the Dx state. Taken together, our findings critically identified a reproducible RT-associated miR-footprint for understanding how RT influences NB biology beyond its established effects on DNA damage and local tumor control.

Among the miRs showing "robust" RT-associated gains (e.g., miR-513a-5p and related family members), studies have indicated roles in restraining proliferation and immune-evasion programs in other malignancies, providing mechanistic plausibility for the observed enrichments [31]. Although this work prioritized a network-level analysis rather than single-miRNA validation, the convergent pathway signatures, spanning DDR, chromatin remodeling, and immune signaling, support a plausible mechanistic chain whereby RT (1) re-activates miRs that throttle oncogenic signaling and repair advantage, (2) shifts EMT→MET, and (3) enhances therapy susceptibility in PD tumors. This complements reports that MYCN/c-MYC, RAD51-mediated repair, and NFκB axes modulate radioresponse and post-RT phenotypes in NB and related models [18,19,22,25,26,32]. Furthermore, this post-transcriptional reprogramming dovetails with known RT effects on tumor cell fate and with our group's prior observations linking RT to NFκB-dependent signaling, invasion dynamics, and metastatic risk modulation, underscoring the need to consider dose, fractionation, and timing as variables that could tune the miRNA response landscape.

Contemporary RT modalities (3D-RT, IMRT and proton therapy) are routinely integrated in consolidation, achieving excellent local control and improved survival in selected series. However, the value of RT in the management of PD has remained under-characterized [10,33,34]. By showing that RT reverses PD-specific miR collapse and activates pro-regression networks that converge on tumor suppression and differentiation, our data provide a molecular rationale for judicious use or intensification of RT in the PD setting. These findings also raise the hypothesis that RT timing (e.g., strategic administration during PD or in maintenance) might preempt or interrupt evolutionary trajectories that otherwise culminate in relapse. In practical terms, this opens the door to miR-informed RT decisions, for example, using a miR-based PD/RT-response score to select candidates for dose escalation, field adaptation (e.g., metastatic foci), or modality selection (proton *vs*. photon) with an eye toward maximizing molecular benefit while minimizing late effects [10,13,33,34,35,36,37].

The translational significance of these findings lies in their clear potential to reshape clinical management of PD-NB. The sharp dichotomy between PD, characterized by global miR loss, and RD-RT, marked by broad miR gain and regulatory reconstitution, indicates that miR signatures could serve as clinically actionable biomarkers for detecting PD evolution and dynamically monitoring RT benefit, including the use of serum-circulating miRs for noninvasive surveillance, an approach supported by prior evidence that circulating miRs track NB progression [35,36,37]. Beyond biomarker applications, the RT-induced restoration of tumor-suppressive miRs opens opportunities for therapeutic synergy, such as combining RT with miR-based therapeutics (mimics or antagomiRs) or pairing RT with DNA-damage–response modulators, including p53 pathway activators or RAD51 inhibitors, to stabilize RT-mediated reprogramming and prevent re-emergence of PD-favoring states; moreover, integrating RT with immunotherapy, such as anti-GD2 or cytokine-supported immune strategies, may be particularly advantageous if RT-activated miRNAs enhance tumor immune visibility [13,18,21,38,39]. Finally, if RT-activated miRs indeed promote differentiation, MET transition, and CSC depletion, then tracking miRNA recovery trajectories could rationally guide refinement of maintenance-phase strategies, including the selective use of post-consolidation maintenance RT, dose-modulated and site-directed approaches, or stereotactic treatment of oligo-progressive lesions, with miRNA signatures informing both continuation and de-escalation decisions in real time [10,13,34,35,39,40]. To that end, histologic comparison of Dx, PD, and RT-RD demonstrates that clinical RT exerts profound effects on tumor architecture, differentiation, and lineage maturation. Dx specimens exhibited moderately differentiated NB, whereas PD tumors displayed poorly differentiated, hypercellular architecture. Following RT, RD tumors showed reduced neuroblast density, expanded neuropil, differentiating neuroblasts, and ganglioneuroma-like maturation, indicating RT-driven differentiation consistent with MET signatures. Multiplex-IF further supports RT-induced reprogramming: PD tumors expressed high SOX2, CD44, Ki-67, and PD-L1 features of plastic, proliferative and immune-evasive CSC-like states. RT curbed SOX2/CD44, reduced Ki-67, induced p53, and dampened PD-L1, aligning with RT-induced miR gains that target CSC maintenance, cell cycle progression, EMT, and immune escape, while activating DDR and immune visibility pathways.

The methodological strengths of this study arise from its design, which compared tumors across Dx, PD, and RD-RT, allowing identification of patient-independent miRNA signatures supported by rigorous FDR-controlled statistical filtering, thus enabling meaningful inference despite the

small cohort size. The use of FFPE-compatible RNA extraction and a uniform microarray platform ensured technical consistency across archival specimens, while the application of miRNA-centric network analytics (miRNet 2.0) provided a system-level interpretation rather than isolated marker identification, allowing molecular patterns to be anchored directly to clinical phenomena such as PD evolution and RT benefit [13,16,35,39].

5. Limitations

Despite the strengths of this study, several important limitations should be considered when interpreting the findings. First, the small sample size (n = 3 per group), retrospective without any longitudinal sampling, single-center design substantially limits statistical power, increase sensitivity to outliers, and restrict the ability to draw patient-independent conclusions. With such limited degrees of freedom, multiple testing correction (e.g., FDR) becomes less stable, and both type I and type II errors remain possible despite the use of stringent effect-size thresholds. Furthermore, although a pairwise traverse analysis was employed to mitigate inter-patient variability by using each patient as their own control, the limited cohort size still constrains robustness and generalizability. An additional limitation is that the PD and RD-RT cohorts were not matched for several potentially important clinical and biological variables, including prior treatment history, timing of tissue acquisition, tumor site, tumor purity, tissue composition, disease status (relapse history), survival outcomes etc. Consequently, some of the observed molecular differences may reflect underlying cohort heterogeneity rather than RT effect alone. Therefore, the RT-associated miR signatures identified here should be considered hypothesis-generating and warrant validation in larger, prospectively collected, clinically matched cohorts. Third, this study relies on FFPE-derived RNA, which is inherently subject to crosslinking, fragmentation, and inter-sample variability in RNA integrity. Although standardized extraction and quality control procedures were applied, such degradation may introduce systematic bias in miRNA detection and quantification. In addition, the lack of cellular deconvolution prevents precise attribution of miRNA expression changes to tumor, stromal, or immune compartments. Fourth, the use of the Human miRNA OneArray® V7 platform (miRBase v18) limits coverage of the contemporary miRNome, excluding newly annotated miRNAs, isomiRs, and low-abundance small RNAs. Consequently, the dataset does not represent a fully comprehensive miRNA landscape by current standards. Relatedly, the findings are based primarily on microarray profiling without orthogonal validation (e.g., qRT-PCR or small RNA sequencing), and therefore should be considered preliminary. Fifth, mechanistic interpretations are inferred from pathway enrichment and network analyses rather than direct functional validation. No gain- or loss-of-function experiments, miRNA-target interaction assays, or *in vivo* validation models (e.g., PDXs or organoids) were performed, limiting causal inference regarding the role of specific miRNAs in regulating DNA damage response, EMT/MET dynamics, stemness, or immune modulation. Sixth, histopathological and imaging-based findings also have inherent limitations. Due to the small number of samples and considerable intratumoral heterogeneity, tumor cell histomorphometric features were unevenly distributed across sections, precluding reliable semi-quantitative assessment (e.g., Shimada grading, neuropil area ratios, or ganglion cell counts). As a result, histological interpretation was limited to qualitative assessment, and standardized region-of-interest-based quantification could not be implemented without introducing sampling bias. Seventh, although mIF analysis was strengthened with quantitative scoring, other aspects of molecular characterization remain limited. For example, the association between miRNA signatures and clinical outcomes such as survival, recurrence, or treatment response was not evaluated, restricting assessment of biomarker potential. Finally, the generalizability of the findings is limited by both clinical and treatment-related factors. The cohort reflects a single radiotherapy regimen (fractionated EBRT, 2400 cGy), and it remains unclear whether similar miRNA remodeling would occur with alternative modalities such as IMRT, proton therapy, or different dose/fractionation strategies. Additionally, the retrospective, single-center nature of the study further constrains extrapolation to broader patient populations.

6. Future Directions

Future studies should address these limitations through prospective, multicenter designs with larger and clinically well-annotated NB cohorts, enabling robust statistical inference, improved control of confounding variables, and correlation of miRNA signatures with clinical outcomes such as survival, recurrence, and treatment response. Longitudinal sampling (pre-, during-, and post-radiotherapy) will be critical to define the temporal dynamics and durability of miRNA remodeling. Orthogonal validation using qRT-PCR, small RNA sequencing, and target gene expression assays will be essential to confirm array-based findings, expand miRNome coverage, and capture newly annotated or low-abundance miRNAs. Integration of spatial transcriptomics, single-cell RNA/miRNA profiling, and cellular deconvolution approaches will further resolve compartment-specific effects within tumor, stromal, and immune populations. Mechanistic studies should prioritize functional validation of high-impact miRNAs through gain- and loss-of-function assays in NB cell lines, organoids, and patient-derived xenograft models, alongside direct validation of miRNA–target interactions (e.g., luciferase reporter assays). Such studies will clarify causal roles in regulating DNA damage response, EMT/MET plasticity, cancer stem cell maintenance, and

immune modulation. Future work should also expand histological and phenotypic analyses using larger and more uniformly sampled tissue cohorts, enabling standardized quantitative assessment of differentiation (e.g., Shimada grading, neuropil metrics) and improved integration with molecular findings. Clinically, these efforts may enable development of miRNA-based biomarkers or composite response scores for stratifying patients and optimizing radiotherapy strategies, including modality selection, dose, and sequencing with systemic therapies. Comparative studies across diverse radiotherapy platforms (e.g., IMRT, proton therapy) and combination regimens (e.g., immunotherapy, DDR inhibitors) will be essential to determine whether the observed miRNA reprogramming is conserved across treatment contexts. Finally, given the importance of survivorship in pediatric oncology, future translational studies should integrate molecular efficacy with toxicity minimization, leveraging miRNA-based readouts to guide precision radiotherapy and identify the lowest effective dose and regimen that achieves durable tumor control while preserving quality of life.

7. Conclusion

Our data reveal the post-transcriptional state transition in HR-NB progression and its modulation by RT. PD is characterized by widespread miR loss, aligning with therapy resistance, stemness, and immune escape; RT produces a broad and conserved miR gain, reversing PD-linked deficits and activating programs consonant with differentiation, apoptosis, and immune engagement. While our findings support a potential RT-associated reprogramming of the NB miRNome, the observed differences between PD and RD-RT tumors should be interpreted cautiously given possible confounding by treatment history, sampling characteristics, tumor composition, and disease status, underscoring the need for validation in larger, prospectively matched cohorts. Overall, this proof-of-concept molecular footprint of RT benefit provides a substrate for deploying RT not only as a local cytotoxic modality, but as a global post-transcriptional reprogrammer of PD biology, an insight with direct implications for biomarker development, treatment sequencing, and rational combination therapy in HR-NB.

Abbreviations

RT, Radiotherapy; CSC, Cancer Stem Cell; EMT, Epithelial to Mesenchymal Transition; FDR, False Discovery Rate; TGFβ, Transforming Growth Factor β; mTOR, mechanistic Target of Rapamycin; ECM, Extra Cellular Matrix; GAG, Glycosaminoglycan; MAPK, Mitogen-activated Protein Kinase; GTP, Guanosine triphosphate; VEGF, Vascular Endothelial Growth factor; EGFR, Epidermal Growth Factor Receptor; ER, Endoplasmic Reticulum; RD, Residual Disease; Dx, Diagnosis; PD, Progressive disease; MET, Mesenchymal to Epithelial Transition; CT, Chemotherapy; IMCT, Intensive Multimodal Clinical Therapy; HR-NB, High Risk Neuroblastoma; 3D RT, Three-Dimensional Photon RT; IMRT, Intensity Modulated RT; PT, Proton Therapy; TD, Total Dose; SCT, Stem Cell Transplantation; EFS, Event Free Survival; OS, Overall Survival; miRNA, microRNA; HR, High-risk; EBRT, External Beam RT; FFPE, Formalin-Fixed Paraffin-Embedded; DEM, Differential Expression miR; miRNome, global miR; H&E, Hematoxylin and Eosin.

Availability of Data and Materials

The datasets used and analyzed during the current study are available from the corresponding author on reasonable request.

Author Contributions

NA contributed to the conception and design of the experiments. SN, PS, SM, SA contributed to biospecimen collection, sectioning, IHC, Multi-Plex IF, image acquisition, digital microscopy, and data interpretation. SM, PS, and SN contributed to miRNome profiling, data acquisition, data analysis. LP, PS, SN contributed to bioinformatics and DEG and gene ontology. All authors read and approved the final manuscript. All authors contributed to editorial changes in the manuscript. All authors have participated sufficiently in the work and agreed to be accountable for all aspects of the work.

Ethics Approval and Consent to Participate

The study was carried out in accordance with the guidelines of the Declaration of Helsinki, and all protocols were approved by the University of Oklahoma Health Sciences Center (OUHSC) (IRB-14601) and Oklahoma State University (OSU) (IRB-23-496) Institutional Review Boards (IRBs), permitting the research use of de-identified human specimens. All experimental procedures adhered to institutional guidelines for the protection of human subjects.

Acknowledgment

Not applicable.

Funding

This work was partially or in full funded by Department of Defense, DoD CA-210339; National Institutes of Health, NIH-P30GM154635; Oklahoma Center for the Advancement of Science and Technology, OCAST-HR19-045 and NIH-NCI- Cancer Center Support Grant, P30CA225520.

Conflicts of Interest

The authors declare no conflicts of interest. Given his role as the Guest Editor, Natarajan Aravindan had no involvement in the peer-review of this article and has no ac-

cess to information regarding its peer review. Full responsibility for the editorial process for this article was delegated to Amancio Carnero Moya.

Declaration of AI and AI-Assisted Technologies in the Writing Process

Open artificial intelligence platform (ChatGPT) was used to generate the graphical abstract. The authors reviewed, edited, and finalized the graphical abstract and take full responsibility for its content.

Supplementary Material

Supplementary material associated with this article can be found, in the online version, at https://doi.org/10.31083/FBL52737.

References

[1] Crane JN, Dagalakis U, Gartrell RD, Schultz KAP, Laetsch TW. Rare but not forgotten: Therapeutic advancements for rare childhood cancers. Molecular Therapy. Oncology. 2025; 33: 201084. https://doi.org/10.1016/j.omton.2025.201084

[2] George NG, Rishi B, Dhanda H, Joseph GT, Swain SK, Kaur M, et al. Pediatric tumor microenvironment: developmental dynamics and therapy resistance. Frontiers in Oncology. 2025; 15: 1663975. https://doi.org/10.3389/fonc.2025.1663975

[3] DuBois SG, Macy ME, Henderson TO. High-Risk and Relapsed Neuroblastoma: Toward More Cures and Better Outcomes. American Society of Clinical Oncology Educational Book. American Society of Clinical Oncology. Annual Meeting. 2022; 42: 768–780. https://doi.org/10.1200/EDBK_349783

[4] Chan GC, Hindsberger C, Morsing A, Lisby S. Naxitamab and granulocyte macrophage colony stimulating factor (GM-CSF) in combination with irinotecan and temozolomide in patients with high-risk neuroblastoma with primary refractory disease or in first relapse: An international, single-arm, multicenter phase 2 trial. Journal of Clinical Oncology. 2022; 40: TPS10061. https://doi.org/10.1200/JCO.2022.40.16_suppl.TPS10061

[5] Richards RM, Sotillo E, Majzner RG. CAR T Cell Therapy for Neuroblastoma. Frontiers in Immunology. 2018; 9: 2380. https://doi.org/10.3389/fimmu.2018.02380

[6] Zhou X, Wang X, Li N, Guo Y, Yang X, Lei Y. Therapy resistance in neuroblastoma: Mechanisms and reversal strategies. Frontiers in Pharmacology. 2023; 14: 1114295. https://doi.org/10.3389/fphar.2023.1114295

[7] Li F, Zhang W, Hu H, Zhang Y, Li J, Huang D. Factors of Recurrence After Complete Response in Children with Neuroblastoma: A 16-Year Retrospective Study of 179 Cases. Cancer Management and Research. 2022; 14: 107–122. https://doi.org/10.2147/CMAR.S343648

[8] Romero LE, Neto IQ, Antunes VL, Rodrigues MM, Mercado JP, Caran EM. 1030P Survival rates in high-risk neuroblastoma patients undergoing anti-GD2 immunotherapy: A single arm meta-analysis and systemic review. Annals of Oncology. 2024; 35: S694–S695. https://doi.org/10.1016/j.annonc.2024.08.1089

[9] Bahmad HF, Chamaa F, Assi S, Chalhoub RM, Abou-Antoun T, Abou-Kheir W. Cancer Stem Cells in Neuroblastoma: Expanding the Therapeutic Frontier. Frontiers in Molecular Neuroscience. 2019; 12: 131. https://doi.org/10.3389/fnmol.2019.00131

[10] Zhao Q, Liu Y, Zhang Y, Meng L, Wei J, Wang B, et al. Role and toxicity of radiation therapy in neuroblastoma patients: A literature review. Critical Reviews in Oncology/hematology. 2020; 149: 102924. https://doi.org/10.1016/j.critrevonc.2020.102924

[11] Jazmati D, Hero B, Thole-Kliesch TM, Merta J, Deubzer HE, Bäumer C, et al. Efficacy and Feasibility of Proton Beam Therapy in Relapsed High-Risk Neuroblastoma-Experiences from the Prospective KiProReg Registry. Current Oncology (Toronto, Ont.). 2022; 29: 8222–8234. https://doi.org/10.3390/curroncol29110649

[12] Gatcombe HG, Marcus RB, Jr, Katzenstein HM, Tighiouart M, Esiashvili N. Excellent local control from radiation therapy for high-risk neuroblastoma. International Journal of Radiation Oncology, Biology, Physics. 2009; 74: 1549–1554. https://doi.org/10.1016/j.ijrobp.2008.10.069

[13] Mestdagh P, Boström AK, Impens F, Fredlund E, Van Peer G, De Antonellis P, et al. The miR-17-92 microRNA cluster regulates multiple components of the TGF-β pathway in neuroblastoma. Molecular Cell. 2010; 40: 762–773. https://doi.org/10.1016/j.molcel.2010.11.038

[14] Aravindan N, Subramanian K, Somasundaram DB, Herman TS, Aravindan S. MicroRNAs in neuroblastoma tumorigenesis, therapy resistance, and disease evolution. Cancer Drug Resistance (Alhambra, Calif.). 2019; 2: 1086–1105. https://doi.org/10.20517/cdr.2019.68

[15] Khan FH, Pandian V, Ramraj S, Aravindan S, Herman TS, Aravindan N. Reorganization of metastamiRs in the evolution of metastatic aggressive neuroblastoma cells. BMC Genomics. 2015; 16: 501. https://doi.org/10.1186/s12864-015-1642-x

[16] Southgate HED, Chen L, Curtin NJ, Tweddle DA. Targeting the DNA Damage Response for the Treatment of High Risk Neuroblastoma. Frontiers in Oncology. 2020; 10: 371. https://doi.org/10.3389/fonc.2020.00371

[17] Berglund H, Salomonsson SL, Mohajershojai T, Gago FJ, Lane DP, Nestor M. p53 stabilisation potentiates [(177)Lu]Lu-DOTATATE treatment in neuroblastoma xenografts. European Journal of Nuclear Medicine and Molecular Imaging. 2024; 51: 768–778. https://doi.org/10.1007/s00259-023-06462-3

[18] Xu Y, Chen K, Cai Y, Cheng C, Zhang Z, Xu G. Overexpression of Rad51 predicts poor prognosis and silencing of Rad51 increases chemo-sensitivity to doxorubicin in neuroblastoma. American Journal of Translational Research. 2019; 11: 5788–5799.

[19] Le Grand M, Mukha A, Püschel J, Valli E, Kamili A, Vittorio O, et al. Interplay between MycN and c-Myc regulates radioresistance and cancer stem cell phenotype in neuroblastoma upon glutamine deprivation. Theranostics. 2020; 10: 6411–6429. https://doi.org/10.7150/thno.42602

[20] Jadhav U, Mohanam S. Response of neuroblastoma cells to ionizing radiation: modulation of in vitro invasiveness and angiogenesis of human microvascular endothelial cells. International Journal of Oncology. 2006; 29: 1525–1531.

[21] Hein AL, Ouellette MM, Yan Y. Radiation-induced signaling pathways that promote cancer cell survival (review). International Journal of Oncology. 2014; 45: 1813–1819. https://doi.org/10.3892/ijo.2014.2614

[22] Ahmed KM, Li JJ. NF-kappa B-mediated adaptive resistance to ionizing radiation. Free Radical Biology & Medicine. 2008; 44: 1–13. https://doi.org/10.1016/j.freeradbiomed.2007.09.022

[23] Ramraj SK, Aravindan S, Somasundaram DB, Herman TS, Natarajan M, Aravindan N. Serum-circulating miRNAs predict neuroblastoma progression in mouse model of high-risk metastatic disease. Oncotarget. 2016; 7: 18605–18619. https://doi.org/10.18632/oncotarget.7615

[24] Subramanian P, Mohanvelu S, Aravindan S, Jahir Hussain AP, Narayanan S, Salim S, et al. Cellular Identity Crisis: RD3 Loss Fuels Plasticity and Immune Silence in Progressive Neuroblastoma. Advanced Science (Weinheim, Baden-Wurttemberg, Germany). 2026; 13: e19586. https://doi.org/10.1002/advs.202519586

[25] Singh J, Thachil T, Misir S, Altay DU, Yaman SO, Singh G, et al. Expression of microRNAs following radiation therapy and association with severity of radiotherapy-induced toxicity among patients with prostate adenocarcinoma: A systematic review and meta-analysis. World Academy of Sciences Journal. 2024; 6: 27. https://doi.org/10.3892/wasj.2024.242

[26] Chen H, Han Z, Luo Q, Wang Y, Li Q, Zhou L, et al. Radiotherapy modulates tumor cell fate decisions: a review. Radiation Oncology (London, England). 2022; 17: 196. https://doi.org/10.1186/s13014-022-02171-7

[27] Qiu B, Matthay KK. Advancing therapy for neuroblastoma. Nature Reviews. Clinical Oncology. 2022; 19: 515–533. https://doi.org/10.1038/s41571-022-00643-z

[28] Guo Q, Yang W, Robinson G, Chaludiya K, Abdulkadir AN, Roy FG, et al. Unlocking the Radiosensitizing Potential of MYC Inhibition in Neuroendocrine Malignancies. International Journal of Radiation Oncology, Biology, Physics. 2025; 122: 1310–1326. https://doi.org/10.1016/j.ijrobp.2025.04.034

[29] Huang RX, Zhou PK. DNA damage response signaling pathways and targets for radiotherapy sensitization in cancer. Signal Transduction and Targeted Therapy. 2020; 5: 60. https://doi.org/10.1038/s41392-020-0150-x

[30] Nickoloff JA, Taylor L, Sharma N, Kato TA. Exploiting DNA repair pathways for tumor sensitization, mitigation of resistance, and normal tissue protection in radiotherapy. Cancer Drug Resistance (Alhambra, Calif.). 2021; 4: 244–263. https://doi.org/10.20517/cdr.2020.89

[31] Chen X, Zhao G, Wang F, Gao F, Luo H, Wang Y, et al. Upregulation of miR-513b inhibits cell proliferation, migration, and promotes apoptosis by targeting high mobility group-box 3 protein in gastric cancer. Tumour Biology : the Journal of the International Society for Oncodevelopmental Biology and Medicine. 2014; 35: 11081–11089. https://doi.org/10.1007/s13277-014-2405-z

[32] Moloudi K, Haghdoost S. An Update on Role of Ionizing Radiation to Enhance Proliferation and Differentiation of Normal Stem Cells via Activation of NRF2 Pathway: Review. Antioxidants (Basel, Switzerland). 2025; 14: 986. https://doi.org/10.3390/antiox14080986

[33] Marinova L, Vassileva V, Petrov V. Palliative 3D conformal radiotherapy of children's neuroblastoma non-resectable liver metastasis: clinical case with literature overview. Journal of Gastroenterology Pancreatology and Hepatobilary Disorders. 2022; 6: 054. https://doi.org/10.31579/2641-5194/054

[34] Ritner C, Popović J, Abouzeid A, Li Y, Paunesku T, Papineni R, et al. Gene Expression and Early Radiation Response of Two Distinct Neuroblastoma Cell Lines. Oncology. 2023; 101: 446–456. https://doi.org/10.1159/000530902

[35] Jonas S, Izaurralde E. Towards a molecular understanding of microRNA-mediated gene silencing. Nature Reviews. Genetics. 2015; 16: 421–433. https://doi.org/10.1038/nrg3965

[36] Smith V, Foster J. High-Risk Neuroblastoma Treatment Review. Children (Basel, Switzerland). 2018; 5: 114. https://doi.org/10.3390/children5090114

[37] Wu L, Chen Z, Zhang J, Xing Y. Effect of miR-513a-5p on etoposide-stimulating B7-H1 expression in retinoblastoma cells. Journal of Huazhong University of Science and Technology. Medical Sciences = Hua Zhong Ke Ji Da Xue Xue Bao. Yi Xue Ying De Wen Ban = Huazhong Keji Daxue Xuebao. Yixue Yingdewen Ban. 2012; 32: 601–606. https://doi.org/10.1007/s11596-012-1004-8

[38] Cellini F, Morganti AG, Genovesi D, Silvestris N, Valentini V. Role of microRNA in response to ionizing radiations: evidences and potential impact on clinical practice for radiotherapy. Molecules (Basel, Switzerland). 2014; 19: 5379–5401. https://doi.org/10.3390/molecules19045379

[39] Roth SA, Knutsen E, Fiskaa T, Utnes P, Bhavsar S, Hald ØH, et al. Next generation sequencing of microRNAs from isogenic neuroblastoma cell lines isolated before and after treatment. Cancer Letters. 2016; 372: 128–136. https://doi.org/10.1016/j.canlet.2015.11.026

[40] Hill-Kayser CE, Tochner Z, Li Y, Kurtz G, Lustig RA, James P, et al. Outcomes After Proton Therapy for Treatment of Pediatric High-Risk Neuroblastoma. International Journal of Radiation Oncology, Biology, Physics. 2019; 104: 401–408. https://doi.org/10.1016/j.ijrobp.2019.01.095